

EPR of Ni^+ centers in RbCaF_3 : Application to the study of the 195-K structural phase transition

R. Alcalá, E. Zorita, and P. J. Alonso

Instituto de Ciencia de Materiales de Aragón, Facultad de Ciencias, Universidad de Zaragoza—Consejo Superior de Investigaciones Científicas, Plaza de S. Francisco s/n, E-50009 Zaragoza, Spain

(Received 4 April 1988)

Three types of Ni^+ centers produced by x-ray irradiation in RbCaF_3 have been studied by EPR spectroscopy. All of them have tetragonal symmetry in the crystal cubic phase and their electronic ground state is the $d_{x^2-y^2}$ orbital. They have been found to be similar to those recently reported in KMgF_3 and K_2MgF_4 . One of them (Ni^+ -I) is placed in the center of an elongated octahedron of six fluorine ions. The other two (Ni^+ -II and Ni^+ -III) are associated with neighboring fluorine vacancies. The use of these centers as probes to study the structural phase transitions in RbCaF_3 has also been investigated. From the tilting of the gyromagnetic tensor of Ni^+ -II centers, the temperature dependence of the order parameter for the 195-K phase transition has been measured and a value of the critical exponent $\beta=0.26$ has been obtained. It has not been possible to get any information about this phase transition from the other Ni^+ centers. The 50-K phase transition has no detectable effect on the EPR spectra of any of the Ni^+ centers. The spin-Hamiltonian parameters for the three Ni^+ centers have been obtained and an estimation of the $\text{Ni}^+—\text{F}^-$ distances has been made using the isotropic part of the superhyperfine interaction parameters.

INTRODUCTION

Although nickel ions are chemically unstable in the monovalent state, Ni^+ can be easily produced in ionic crystals by x-ray irradiation of nickel-doped samples. Several Ni^+ centers of tetragonal or near tetragonal symmetry have been reported in different ionic crystals.¹⁻⁵ In these centers Ni^+ ions are either in a distorted octahedral environment or associated with nearby intrinsic defects, and both d_{z^2} and $d_{x^2-y^2}$ orbitals have been found as ground states.

Recently, we reported on an EPR study of tetragonal Ni^+ centers formed by x-ray irradiation in KMgF_3 (Ref. 6) and K_2MgF_4 (Ref. 7). In each of these crystals three different types of Ni^+ centers have been found, all of them with the $d_{x^2-y^2}$ ground state. The models proposed for these defects, which are the same in both compounds, consist of a Ni^+ ion in an elongated octahedron of fluorines for one of the types (Ni^+ -I), while the other two (Ni^+ -II and Ni^+ -III) involve one and two nearest-neighbor fluorine vacancies, respectively. Some information about the relaxation of Ni^+ environments in these centers has been derived by using a slightly modified overlap model proposed by Barriuso and Moreno⁸ to account for the values of Ni^+ fluorine superhyperfine (SHF) interaction parameters.

In this paper we present the extension of these studies to x-ray irradiated $\text{RbCaF}_3:\text{Ni}$ crystals. Three types of Ni^+ centers similar to those found in KMgF_3 and K_2MgF_4 have been observed by EPR. The $\text{Ni}^+—\text{F}^-$ distances have been obtained from the analysis of the shf constants and compared with those derived in Refs. 6 and 7. The results are in agreement with the increase of the

divalent cation-fluorine distance going from KMgF_3 and K_2MgF_4 to RbCaF_3 .

Besides this, we have used the Ni^+ defects as a probe to investigate the RbCaF_3 structural phase transition. It is well known that RbCaF_3 undergoes at least two phase transformations at about 195 and 50 K. The high-symmetry crystal structure is the cubic perovskite. The 195-K transition consists of a rotation of the anion octahedra around one of the cubic $\langle 100 \rangle$ directions and an elongation of the cubic unit cell along the rotation axis. In the 50-K transition the rotation takes place around the $\langle 110 \rangle$ cubic axes. These transitions have already been studied by several techniques, such as neutron^{9,10} and x-ray diffraction,^{10,11} Raman scattering,¹²⁻¹⁴ calorimetry,¹⁵ Mössbauer,^{10,16} etc., as well as NMR (Ref. 17) and EPR techniques. In particular, the 195-K phase transition has been followed by EPR using different paramagnetic probes.¹⁸⁻²² In one of these papers²⁰ the use of Ni^+ ions to investigate the phase transitions has been proposed. Although the values of the rotation angle, which is the order parameter of the transition, are different for the different paramagnetic probes, the critical exponent obtained in all the cases for temperatures close to the phase transition seems to be the same for all of them. In our case, only Ni^+ -II has proved to be sensitive enough to study the 195-K phase transition, while no effects on the EPR spectra of any of the Ni^+ centers have been observed when the crystals were cooled below 50 K. The tilting angles calculated from the orientation of the principal axis of the g tensor have been found to be smaller than the intrinsic ones, but the critical exponent obtained from the temperature dependence of the order parameter between T_c and $T_c - 20$ K is in good agreement with those previously reported in the literature.

EXPERIMENTAL TECHNIQUES

Single crystals of RbCaF₃ nominally doped with 0.5 mol % of NiF₂ were grown at the University of Paderborn by the Bridgman technique using vitreous carbon crucibles. When the samples are cooled down below 195 K, polydomains are usually obtained with the domain axes along the three $\langle 100 \rangle$ cubic directions. Nearly mono-domain samples can be achieved by introducing a cylinder-shaped crystal with a $\langle 100 \rangle$ direction along the cylinder axis into a Teflon coat, the domain orientation then being parallel to that of the cylinder. X-ray irradiation was performed using a normal focus Cu-target tube working at 45 kV and 30 mA. EPR spectra were recorded on a Varian E-112 spectrometer working in the X band. Measurements at 77 K were performed using a quartz immersion Dewar, while a variable-temperature accessory Varian E-257 and a continuous-flow helium cryostat (ESR-900 from Oxford Instruments) were used for temperatures between 10 and 300 K (with a stability of ± 2 K). Magnetic-field values were determined with a Bruker NMR ER035M gaussmeter and the microwave frequency was determined using the diphenylpicrylhydrazyl (DPPH) EPR signal.

EXPERIMENTAL RESULTS

Room-temperature (RT) x-ray irradiation induces new signals at $g \approx 2.6$ and 2.1 in the EPR spectra of these crystals. We show in Fig. 1 the spectrum measured at 230 K (above T_c) with the magnetic field parallel to a $\langle 100 \rangle$ direction, of a RT x-ray irradiated sample. The radiation-induced signals are very similar to those associated with Ni⁺-II and Ni⁺-III centers in x-ray irradiated KMgF₃:Ni, and we will label them in the same way. The lines corresponding to each of these two centers can only be partially resolved in the low-field part of the spectrum (see Fig. 1). The signal corresponding to Ni⁺-II centers shows a well-resolved five-line shf pattern that indicates a shf interaction with four fluorine nuclei, equivalent for this magnetic field orientation. The weaker signal, labeled Ni⁺-III, is strongly overlapped with the Ni⁺-II signal; but from the splitting between the lines that can be observed and the comparison with the results in Ref. 6 we propose that it also consists of five shf lines.

The angular evolution of the Ni⁺-II signal when the magnetic field is rotated in a (100) plane shows that the symmetry of the Ni⁺-II center is tetragonal with the C_4 axis parallel to a $\langle 100 \rangle$ direction. The four fluorine nu-

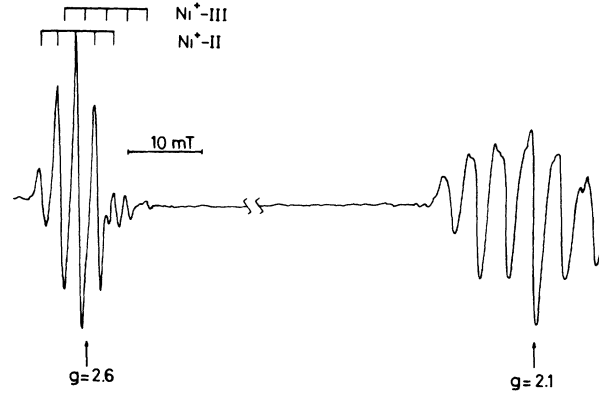


FIG. 1. Ni⁺-II and Ni⁺-III EPR signals created by RT x-ray irradiation in a RbCaF₃:Ni crystal measured at 230 K with the magnetic field parallel to a $\langle 100 \rangle$ direction.

clei responsible for the shf interaction are placed in the corners of a square perpendicular to the tetragonal axis. Unfortunately, the Ni⁺-III signal is too weak to follow its angular evolution.

In order to describe these EPR signals, the following spin Hamiltonian has been used:

$$H = \mu_B (g_x S_x B_x + g_y S_y B_y + g_z S_z B_z) + \sum_{k=1}^4 A_{\perp} (S_{x_k} I_{x_k}^k + S_{y_k} I_{y_k}^k) + A_{\parallel} S_{z_k} I_{z_k}^k, \quad (1)$$

where μ_B is the Bohr magneton, $S = \frac{1}{2}$, $I^k = \frac{1}{2}$, and the z_k axes are parallel to the Ni⁺—F⁻ bonding line, the summation being extended to the four fluorines in the plane perpendicular to the tetragonal axis. The spin-Hamiltonian parameters which give the best fit between calculated and experimental line positions are given in Table I. For the Ni⁺-III center only the values of A_{\perp} and g_{\parallel} ($=g_z$) can be determined from our data.

When the RT irradiated samples are measured at temperatures below 65 K a new EPR signal, due to a different type of Ni⁺ center, is observed. On the other hand, this type of Ni⁺ center is the only one detected in liquid-nitrogen-temperature (LNT) irradiated samples. The EPR spectrum of this center measured at 30 K in a polydomain sample (see the following) with the magnetic field parallel to one of the cubic $\langle 100 \rangle$ directions is given in Fig. 2. Similar behavior has also been found in KMgF₃.⁶ The superhyperfine structure indicates an in-

TABLE I. Values for the spin-Hamiltonian parameters of the different Ni⁺ centers in RbCaF₃. The superhyperfine constants are given in MHz. Primed values correspond to the two axial fluorines.

Center	Temp. (K)	g_x	g_y	g_z	A_{\parallel}	A_{\perp}	A'_{\parallel}	A'_{\perp}
Ni ⁺ -I	30		2.133	2.778	203	88	24	37
Ni ⁺ -II	230		2.115	2.688	221	90		
Ni ⁺ -II (tetrag.)	77		2.114	2.663	233	94		
Ni ⁺ -II (orth.)	77	2.111	2.121	2.672	232	93		
Ni ⁺ -III	230			2.651		98		

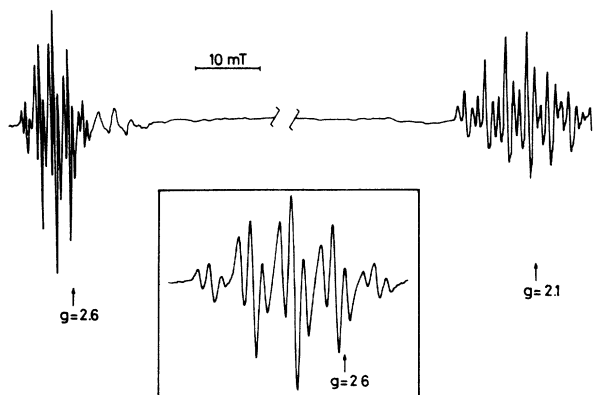


FIG. 2. Ni^{I} EPR signal created by LNT x-ray irradiation in a $\text{RbCaF}_3\text{:Ni}$ crystal measured at 30 K in a polydomain sample with the magnetic field parallel to a pseudocubic $\langle 100 \rangle$ direction. The boxed inset shows a detailed view of the $g=2.6$ region.

teraction with four equivalent fluorine nuclei, but now in each shf line a further splitting is resolved that can be understood as due to a weaker shf interaction with two other equivalent fluorine nuclei. From the angular evolution of this signal we conclude that the Ni^{I} ion is located in a tetragonal environment with four equivalent fluorine ions placed in the plane perpendicular to the tetragonal axis while the two remaining fluorines are symmetrically located along the tetragonal axis. To describe the EPR signal of this new center the following term has been added to the former spin Hamiltonian [Eq. (1)]:

$$\sum_{i=1}^2 A'_{\perp} (S_x I_x^i + S_y I_y^i) + A'_{\parallel} S_z I_z^i, \quad (2)$$

where the z axis is parallel to the tetragonal axis. Again the values of the spin-Hamiltonian parameters are given in Table I.

We will now describe the effects of the phase transitions on the Ni^{I} EPR signals. As mentioned above RbCaF_3 undergoes two structural phase transitions at about 195 and 50 K. However, we have not been able to observe any change in the EPR signals of Ni^{I} ions that can be associated with the 50 K transition and so we restrict our comments, from now on, to the 195 K transition.

If the EPR spectrum is measured at 77 K (below T_c) in a polydomain sample, some changes occur in the Ni^{II} EPR signal which are more readily seen in the low-field part of the spectrum [Figs. 3(a) and 3(b)]. Each line of the superhyperfine pattern undergoes a further splitting. This splitting can be understood as follows. As we have already said, the 195-K phase transition is accompanied by an elongation of the crystal unit cell one of the $\langle 100 \rangle$ cubic axes and a rotation of the fluorine octahedra along these axes. In a polydomain sample the centers with the tetragonal axis parallel to the domain direction will remain tetragonal, while for those whose tetragonal axis is perpendicular to the domain axis, the local symmetry will be reduced to orthorhombic (see Fig. 4). The split-

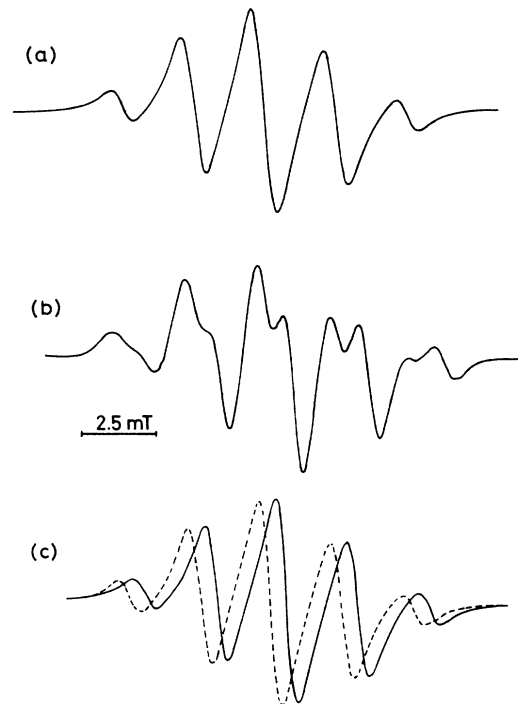


FIG. 3. Low-field group of the Ni^{II} EPR signal with the magnetic field parallel to a $\langle 100 \rangle$ direction (a) measured at 230 K; (b) measured at 77 K in a polydomain sample; (c) measured at 77 K in a monodomain sample with the magnetic field parallel (— —) and perpendicular (—) to the domain orientation.

ting observed in the low-field part of the spectrum is due to different g_z values (the z axis of the center has been taken in the direction of the tetragonal or pseudotetragonal axis) for these two types of centers (the effect of the small rotation of the g tensor on the spectrum of the orthorhombic center appears to be negligible because for this orientation of the magnetic field we are close to a turning point). This fact is confirmed when the EPR spectra measured in a monodomain sample are considered. Figure 3(c) shows the low-field part of the Ni^{II} EPR signal in a monodomain sample measured at 77 K with the magnetic field parallel and perpendicular to the domain axis. The signals corresponding to both centers can be separately observed. The spin-Hamiltonian parameters corresponding to the tetragonal and orthorhombic Ni^{II} centers can be measured in the following way: The g_z values can be determined in a monodomain sample in the low-field part of the spectrum when the magnetic field is parallel (for the tetragonal centers) and perpendicular (for the orthorhombic centers) to the domain orientation. In this last case the small tilting angle has been taken into account. In the high-field region the parameters g_y for both centers can be measured simultaneously when the magnetic field is perpendicular to the domain axis; with \mathbf{B} parallel to the domain orientation the g_x value for the orthorhombic center can be measured from the high-field part of the spectrum. The corresponding results are given in Table I.

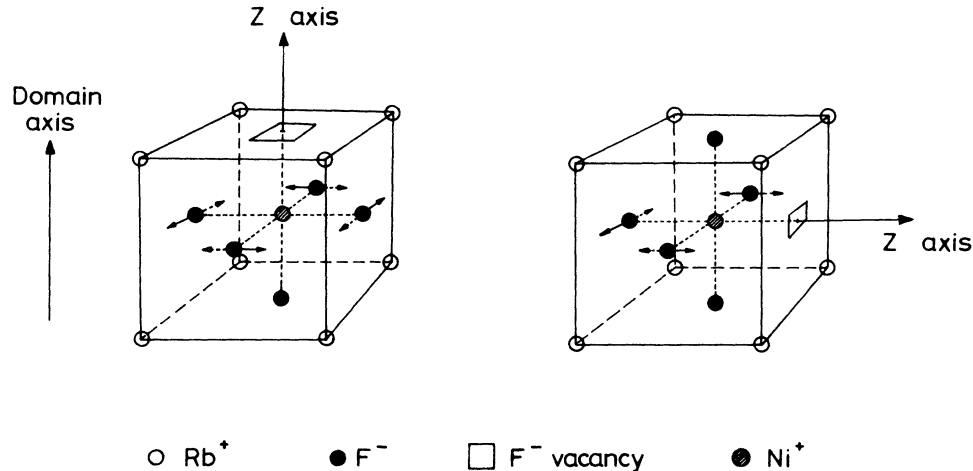


FIG. 4. Schematic representation of the models for the tetragonal (a) and orthorhombic (b) Ni²⁺-II centers in RbCaF₃ below T_c . The two possible directions of rotation for the fluorine octahedra around the domain axis are depicted.

Besides this, and due to the rotation of the fluorine octahedra, the principal axes of the g tensor of the orthorhombic Ni²⁺-II centers are tilted away from the cubic $\langle 100 \rangle$ directions, while for the tetragonal center the orientation of the g tensor remains unaltered. The superhyperfine tensor will follow the tilting of the neighboring fluorine nuclei. However, the observed superhyperfine interaction is too isotropic to observe a small tilting in the orientation of the shf tensor (see Table I), and, in fact, no difference in the superhyperfine interaction has been experimentally observed between cubic and distorted phases.

To study the phase transition we have measured the angle of tilting of the g tensor in the orthorhombic Ni²⁺-II center. This has been performed by measuring the evolution of the EPR signal in a monodomain sample when the magnetic field is rotated in a (001) plane perpendicular to the domain axis. When the magnetic field lies along a cubic $\langle 100 \rangle$ direction the Ni²⁺-II centers whose z axis is nearly parallel to the magnetic field are equivalent, since some of them have their axis rotated "clockwise" and others "counterclockwise" (see Fig. 4). When the magnetic field departs from the $\langle 100 \rangle$ direction these centers will become inequivalent and the EPR signal will split, as is experimentally observed. We show in Fig. 5 the EPR spectrum corresponding to these centers measured at 77 K with the magnetic field 8° away from a $\langle 100 \rangle$ direction. The spectrum of Ni²⁺-II in KMgF₃, which does not undergo a phase transition, is also given for comparison [Fig. 5(c)]. The splitting between the signals corresponding to centers which have rotated in opposite directions is clearly seen. However, there is a strong overlap between the two signals. Because of this, and in order to determine the tilting angle, a simulation of the spectra corresponding to different tiltings has been performed. The best agreement, that which is shown in Fig. 5(b), corresponds to an angle of about 2.4° at LNT. The high-field part of the EPR spectrum contains the sig-

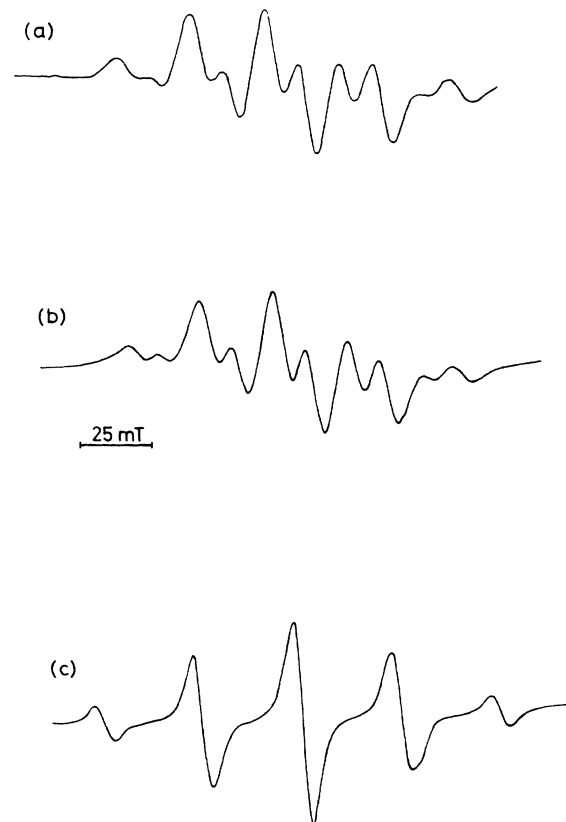


FIG. 5. (a) Low-field group of the orthorhombic Ni²⁺-II EPR signal measured at 77 K with the magnetic field 8° away from the $\langle 100 \rangle$ direction. (b) Simulation of the low-field EPR signal of two Ni²⁺-II centers whose z axes are tilted by $8^\circ - 2.4^\circ = 6.6^\circ$ and $8^\circ + 2.4^\circ = 10.4^\circ$ from the magnetic-field orientation using the spin-Hamiltonian parameters given in Table I for the orthorhombic Ni²⁺-II center at 77 K. (c) Low-field Ni²⁺-II EPR signal in KMgF₃ measured at 77 K with B 8° away from the $\langle 100 \rangle$ direction.

nals due to both orthorhombic and tetragonal Ni^{+II} centers, and therefore the effect of the phase transition is much more difficult to observe.

The angle of tilting can be more accurately estimated by considering the EPR spectrum with the magnetic field parallel to a cubic $\langle 110 \rangle$ direction and also perpendicular to the domain axis. In this direction the signal corresponding to the orthorhombic Ni^{+II} centers whose z axes lie at nearly 45° from the magnetic field is observed in the low-field part of the spectrum. This is the situation at which the line positions are most sensitive to the orientation of the g tensor with respect to the magnetic field, and it has been used to study the evolution of the angle of tilting with temperature. In the cubic phase the centers whose z axes lie at 45° of the magnetic field are magnetically equivalent. Below T_c , due to the tilting of the fluorine octahedra, the angle between the z axis of these centers and the magnetic field becomes larger or smaller depending on the direction of the rotation [Fig. 6(a)]. Thus, the signals corresponding to these centers split when cooling the sample below T_c , as is shown in Fig. 6(c). Measuring this splitting, the rotation angle can be easily calculated, with an estimated accuracy of about

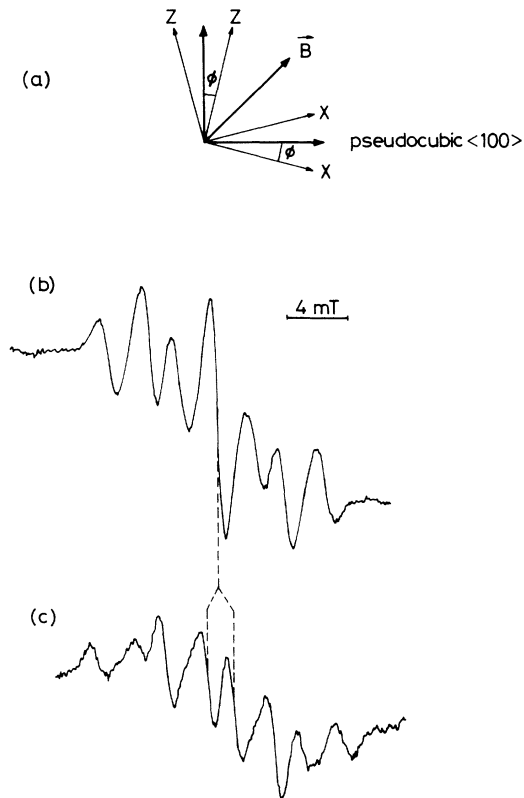


FIG. 6. (a) Relative orientations of the magnetic field and the tilted z axes of the Ni^{+II} orthorhombic centers that have been used to measure the tilting angle ϕ below T_c . The domain orientation is perpendicular to the paper plane, (b), and (c) Ni^{+II} EPR signal corresponding to the above-mentioned situation measured (b) above T_c and (c) at just below T_c . The splitting of the central line is indicated by dashed lines.

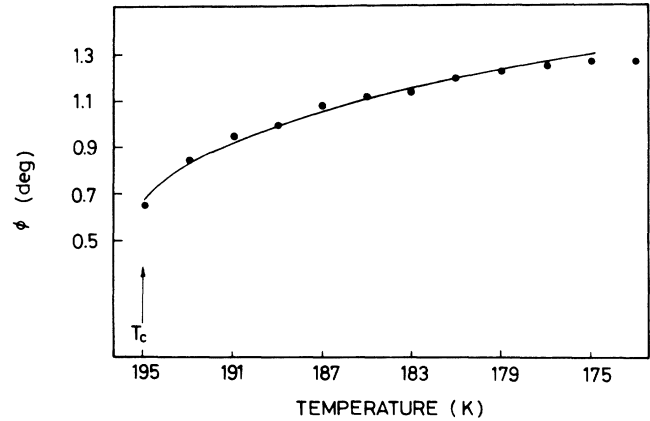


FIG. 7. Dots represent the temperature evolution of the tilting angle of the g tensor of the Ni^{+II} orthorhombic centers. The continuous line corresponds to the expression $\phi = \phi_0 |T - T_0|^\beta$ with $\beta = 0.26$, $T_0 = 203$ K.

0.1° . Figure 7 shows the values obtained in this way as a function of temperature. A discontinuity of 0.7° is observed at T_c , corresponding to the first-order component of the phase transition. Between T_c and $T_c - 20$ K the evolution of the angle of tilting can be fitted to the power law $\phi = \phi_0 |T - T_0|^\beta$, with $T_0 = 202$ K and $\beta = 0.26$.

We have also measured the temperature evolution of the spin-Hamiltonian parameters for both the tetragonal and orthorhombic Ni^{+II} centers between T_c and 30 K. The superhyperfine parameters show no evolution within experimental accuracy in this temperature range. With respect to the gyromagnetic tensor, the most significant variation is observed in the g_z parameter for both tetragonal and orthorhombic centers. This evolution is represented in Fig. 8. As a comparison, the data corresponding to Ni^{+II} centers in KMgF_3 are also included.

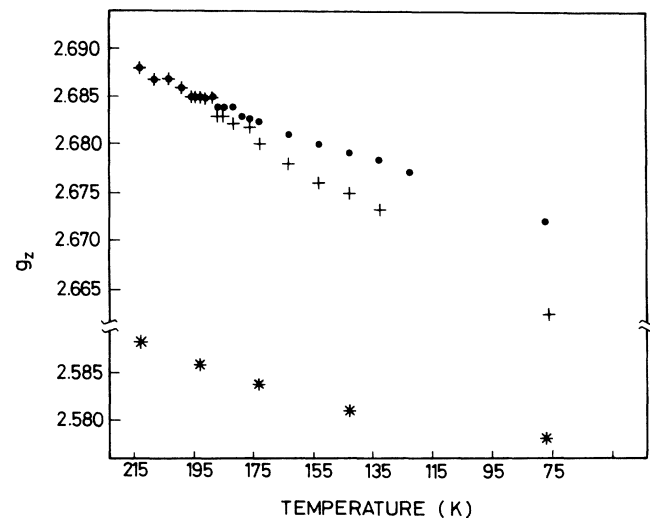


FIG. 8. Temperature evolution of the g_z values for the tetragonal (+) and orthorhombic (●) Ni^{+II} centers. The values for the Ni^{+II} centers in KMgF_3 (*) are also shown for comparison.

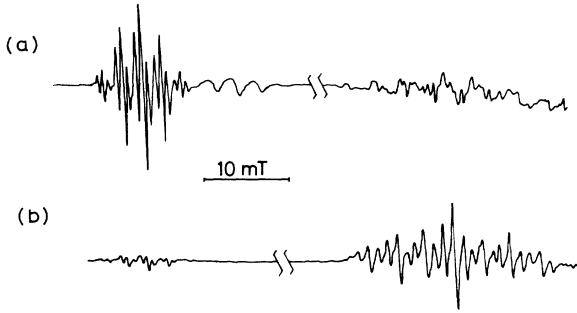


FIG. 9. Ni⁺-I EPR signals in RbCaF₃:Ni measured at 30 K in a monodomain sample with the magnetic field along a pseudocubic $\langle 100 \rangle$ direction and (a) parallel and (b) perpendicular to the domain orientation.

With respect to the Ni⁺-I centers in RbCaF₃, it is noteworthy that only those with their z axis parallel to the domain direction are present below T_c . This can be seen in Fig. 9, where we show the EPR spectrum of a monodomain sample x-ray irradiated at LNT and measured at 30 K with the magnetic field perpendicular [Fig. 9(a)] and parallel [Fig. 9(b)] to the domain orientation. It is clearly seen that most of the centers have the tetragonal axis in the domain direction. Centers whose tetragonal axis is apparently perpendicular to the domain direction can also be seen. This is because the sample is never 100% monodomain.

DISCUSSION

We have essentially described three types of Ni⁺ centers created by x-ray irradiation in RbCaF₃. Their EPR signals are very similar to those found in KMgF₃. The values of the g factors ($g_{zz} > g_{xx}, g_{yy} > g_e$) for all the centers indicate that the unpaired electron is located in a $d_{x^2-y^2}$ orbital. This orbital has its four lobes pointing towards four fluorine nuclei located in a plane perpendicular to the tetragonal axis. This explains the main superhyperfine structure observed in all the Ni⁺ signals. The extra superhyperfine structure observed in the Ni⁺-I signal is due to two fluorine nuclei located along the tetragonal axis. The lack of this structure in the Ni⁺-II and Ni⁺-III centers can be explained assuming that some vacancies are associated with these centers. In KMgF₃ this assumption was supported by bleaching experiments in which a correlation between the growth of the Ni⁺-II EPR signal and the destruction of the F -center absorption band was found. To our knowledge, the optical absorption bands of the different intrinsic defects have not been yet identified in RbCaF₃, and a similar correlation cannot be carried out in a straightforward way. However, because of the similarity between the results obtained in RbCaF₃ and KMgF₃ we assign Ni⁺-II and Ni⁺-III centers to a Ni⁺ ion with one (Ni⁺-II) and two (Ni⁺-III) nearest-neighbor fluorine vacancies placed along the tetragonal axis.

The Ni⁺-I center in KMgF₃ has been associated with Ni⁺ ions in a Jahn-Teller elongated fluorine octahedron.

In RbCaF₃ the Ni⁺-I signal has only been observed below 65 K and so an additional distortion due to the phase transition will also be present. For Cu²⁺ in RbCdCl₃, which undergoes a phase transition at 385 K similar to the one at 195 K in RbCaF₃, it has been shown²³ that the tetragonal distortion is mainly due to a static Jahn-Teller effect. We tentatively propose that the same happens in our case. On the other hand, the fact that only centers with the tetragonal axis parallel to the domain orientation are observed in the monodomain sample can be associated with the additional tetragonal distortion due to the 195-K phase transition.

With respect to the values of the shf interaction parameters corresponding to the four fluorines that cause the main shf structure in the Ni⁺-I and Ni⁺-II signals, we can analyze them using the same procedure given in Ref. 7 in order to obtain some information about the distortions caused by the Ni⁺ ions in the surrounding fluorine octahedra. Since this method has already been described in a more detailed way elsewhere,⁷ only the main ideas are quoted here. In a molecular orbital calculation the NiF₄ cluster wave function can be written as

$$\psi_{x^2-y^2} = N(\phi_{x^2-y^2} - \lambda_{1s}\chi_{1s} - \lambda_{2s}\chi_{2s} - \lambda_{2p}\chi_{2p}), \quad (3)$$

where $\chi_{1s}, \chi_{2s}, \chi_{2p}$ are suitable linear combinations of ligand orbitals. In a purely ionic bonding approximation the mixing coefficients are given by

$$\begin{aligned} \lambda_{1s} &= \sqrt{3} \langle 1s | d_\sigma \rangle, \\ \lambda_{2s} &= \sqrt{3} \langle 2s | d_\sigma \rangle, \\ \lambda_{2p} &= \sqrt{3} \langle 2p | d_\sigma \rangle. \end{aligned} \quad (4)$$

As shown in Ref. 7, when covalency effects are introduced in an approximate way the isotropic part of the superhyperfine interaction can be written as

$$a = \frac{8\pi}{3} g_e \mu_e g_N \mu_N \left| \frac{1}{2} \sqrt{3} c \langle 2s | d_\sigma \rangle \phi(0) \right|^2, \quad (5)$$

where a value of $c=1.1$ has been used for Ni⁺ in KMgF₃ and K₂MgF₃. The overlap integral can be evaluated using Clementti and Roetti atomic wave functions²⁴ and then expression (5) gives a relation between the isotropic superhyperfine constant and the Ni⁺-F⁻ distance. Using this procedure the values we have obtained for this distance in RbCaF₃ are 2.21 Å for Ni⁺-I and 2.17 Å for Ni⁺-II centers. These distances are slightly larger than those found in KMgF₃ and K₂MgF₃. This can be understood because of the larger distance between the divalent cation and the fluorine in RbCaF₃ as compared with the two magnesium compounds.

We will now discuss the information that can be obtained on the 195-K phase transition of RbCaF₃ using the changes observed in the Ni⁺ EPR signals. No changes have been detected in the superhyperfine parameters of Ni⁺-II when the crystal is cooled down below T_c . On the other hand, it can be easily estimated that a rotation of a few degrees around the domain axis will have no effect on the shf structure within experimental accuracy because of the small anisotropy of the shf tensor for both Ni⁺-I and Ni⁺-II centers.

We are then left with the orientation of the g tensor. Since Ni^+ -I centers are tetragonal with the fourfold axis along the domain orientation, it is clear that the tilting around this axis, which appears below 195 K, does not produce any change in the orientation of the g tensor. Consequently, these centers are not useful for measuring the tilting angle. The same thing happens with the Ni^+ -II ions having the tetragonal axis parallel to the domain orientation.

In the case of Ni^+ -II ions which become orthorhombic below T_c , the tilting of the fluorine ions around the domain axis (which corresponds to either the x or y axis of the center) induces a rotation of the g tensor and, as we have previously explained, the tilting angle that corresponds to the order parameter of the transition can be obtained from our EPR measurements.

The angles of tilting obtained with this method are much smaller than the intrinsic ones measured by neutron diffraction or even those measured with other EPR probes [for example, the intrinsic value at LNT is about 7° ,¹⁰ compared with 2.4° reported in this paper, and the first-order contribution given in Ref. 10 amounts to about 2.7° while our EPR measurements yield only 0.7°]. There are several reasons that can contribute to this fact. It is known that because of the distortion induced by the paramagnetic probes the angles of tilting obtained by EPR are usually smaller than the intrinsic ones. Besides this, in the case of the orthorhombic Ni^+ -II centers, one of the four fluorines that normally rotates is missing (see Fig. 4), and this can influence the rotation angle. Finally, we should mention that we are measuring the orientation

of the g tensor and its principal directions are determined not only by the rotating fluorines, but also by the Rb^+ ions that do not rotate.

Although the absolute values of the rotation angles are smaller than the intrinsic ones, the critical exponent we have obtained ($\beta=0.26$) agrees quite well with the ones measured by other techniques. For example, neutron diffraction studies yield $\beta=0.25$, which agrees with Mössbauer experiments^{10,17} and single crystal x-ray diffraction,¹¹ NMR spectroscopy²¹ yields $\beta=0.27$, while optical birefringence¹⁴ and Raman scattering¹³ yield somewhat higher values: $\beta=0.29$ and $\beta=0.33$, respectively.

Finally, with respect to the temperature dependence of the g factors, previous neutron diffraction experiments⁹ have found a minimum of the Ca—F bond length at $T=T_c$, for both equatorial and axial fluorines. This evolution should be reflected somehow in the value of the g parameters since they are affected by the energy difference between the $d_{x^2-y^2}$ ground state and excited states, which is governed by the crystal field strength and consequently by the Ni^+ — F^- distances. However, none of this kind is experimentally observed. This shows again that Ni^+ ions are not very sensitive to the 195-K phase transition in RbCaF_3 .

ACKNOWLEDGMENT

We are indebted to Professor Spaeth [University of Paderborn, Federal Republic of Germany (FRG)], who kindly provided the $\text{RbCaF}_3:\text{Ni}$ crystals.

- ¹P. J. Alonso, J. Casas-González, H. W. den Hartog, and R. Alcalá, *Phys. Rev. B* **27**, 2722 (1983).
- ²P. J. Alonso, J. Casas-González, H. W. den Hartog, and R. Alcalá, *J. Phys. C* **16**, 3523 (1983).
- ³W. Hayes and J. Wilkens, *Proc. R. Soc. London* **A281**, 340 (1964).
- ⁴A. Schoenberg, J. T. Suss, Z. Luz, and W. Low, *Phys. Rev. B* **9**, 2047 (1974).
- ⁵J. J. Rousseau, M. Binois, and F. C. Fayet, *C. R. Acad. Sci.* **B279**, 1079 (1974).
- ⁶E. Zorita, P. J. Alonso, and R. Alcalá, *Phys. Rev. B* **35**, 3116 (1987).
- ⁷R. Alcalá, E. Zorita, and P. J. Alonso, *J. Phys. C* **21**, 461 (1988).
- ⁸M. T. Barriuso and M. Moreno, *Phys. Rev. B* **29**, 3623 (1984).
- ⁹J. Maetz, M. Muellner, and J. Jex, *Phys. Status Solidi A* **50**, K117 (1978).
- ¹⁰H. Jex, J. Maetz, and M. Muellner, *Phys. Rev. B* **21**, 1209 (1980).
- ¹¹J. Maetz, M. Muellner, H. Jex, and K. Peters, *Solid State Commun.* **28**, 555 (1978).
- ¹²A. J. Rushworth and J. F. Ryan, *Solid State Commun.* **18**, 1239 (1976).

- ¹³C. Ridou, M. Rousseau, J. Y. Gesland, J. Nouet, and A. Zazembowitch, *Ferroelectrics* **12**, 199 (1976).
- ¹⁴J. B. Bates, R. W. Major, and F. A. Modine, *Solid State Commun.* **16**, 1347 (1975).
- ¹⁵J. C. Ho, *Phys. Rev. B* **13**, 447 (1975).
- ¹⁶J. Maetz, N. M. Butt, H. Jex, and M. Muellner, *Phys. Lett.* **68A**, 87 (1978).
- ¹⁷S. V. Bhat and P. P. Mahendroo, *Phys. Rev. B* **20**, 1812 (1979).
- ¹⁸J. J. Rousseau, M. Rousseau, and F. C. Fayet, *Phys. Status Solidi B* **73**, 625 (1976).
- ¹⁹F. A. Modine, E. Sonder, and W. P. Unruh, *Phys. Rev. B* **10**, 1623 (1974).
- ²⁰J. J. Rousseau, A. Leble, J. Y. Buzaré, and J. C. Fayet, *Ferroelectrics* **12**, 201 (1975).
- ²¹L. E. Halliburton and E. Sonder, *Solid State Commun.* **21**, 445 (1977).
- ²²J. Y. Buzaré, M. Fayet-Bonnell, and J. C. Fayet, *J. Phys. C* **13**, 857 (1980).
- ²³A. E. Usachev and Yu. V. Yablokov, *Fiz. Tverd. Tela (Leningrad)* **22**, 260 (1980) [*Sov. Phys. Solid State* **22**, 153 (1980)].
- ²⁴E. Clementi and C. Roetti, *At. Data Nucl. Data Tables* **14**, 177 (1974).